University of Reading

Key physicochemical parameters influencing reactive species in Plasma-Processed-Air (PPA) originated from microwave discharge

Article

Published Version

Creative Commons: Attribution-Noncommercial-No Derivative Works 4.0

Open Access

Yijiao, Y., Weihe, T., Stachowiak, J., Ehlbeck, J., Schnabel, U. and Karatzas, K.-A. (2026) Key physicochemical parameters influencing reactive species in Plasma-Processed-Air (PPA) originated from microwave discharge. Plasma Processes and Polymers, 23 (1). e70092. ISSN 1612-8869 doi: 10.1002/ppap.70092 Available at https://centaur.reading.ac.uk/127156/

It is advisable to refer to the publisher's version if you intend to cite from the work. See Guidance on citing.

To link to this article DOI: http://dx.doi.org/10.1002/ppap.70092

Publisher: Wiley

All outputs in CentAUR are protected by Intellectual Property Rights law, including copyright law. Copyright and IPR is retained by the creators or other copyright holders. Terms and conditions for use of this material are defined in the End User Agreement.

University of Reading

www.reading.ac.uk/centaur

CentAUR

Central Archive at the University of Reading

Reading's research outputs online

Check for updates

Plasma Processes and Polymers

PLASMA PROCESSES AND POLYMERS

RESEARCH ARTICLE OPEN ACCESS

Key Physicochemical Parameters Influencing Reactive Species in Plasma-Processed-Air (PPA) Originated From Microwave Discharge

Yijiao Yao[1,2] | Thomas Weihe[2] | Jörg Stachowiak[2] | Jörg Ehlbeck[2] | Uta Schnabel[2] | Kimon-Andreas Karatzas[1]

[1]Department of Food & Nutritional Sciences, University of Reading, Reading, UK | [2]Department of Plasma Biotechnology, Leibniz Institute for Plasma Science and Technology, Greifswald, Germany

Correspondence: Uta Schnabel (uta.schnabel@inp-greifswald.de)

Received: 21 May 2025 | **Revised:** 6 October 2025 | **Accepted:** 22 October 2025

Funding: This study is part of the TRANSIT project and has received funding from the European Union's Horizon 2020 research and innovation program under the Marie Skłodowska-Curie grant agreement N°955431.

Keywords: ambient air plasma | FT-IR | nitrogen oxides | non-thermal plasma | SIE

ABSTRACT

Fourier transformation infrared (FTIR) spectroscopy was used to identify the antimicrobial chemical composition of plasma processed air (PPA) generated by a microwave plasma source—MidiPLexc. NO was found to be the first product with maximum concentration of 1030 ppm. NO_2 was the dominant long-living species with maximum concentration of 10 520 ppm, which was in equilibrium with its dimer—N_2O_4. Key physicochemical parameters influencing the concentrations were identified. Elevated input power mainly promoted NO_2 generation and 1.5 SLM was determined to be the critical flow rate for the maximum NO_2 yield. NO_2 concentration was reduced by 40% under humid condition with 50 W power input. A prediction model of NO_x generation was made based on specific input energy (SIE).

1 | Introduction

The increasing demand for healthy lifestyle and better diet has led to a growing interest in fresh or minimally processed food products [1]. However, the raw materials of these products are prone to contamination by harmful microbes and pathogens, including *Escherichia coli* O157:H7, *Listeria monocytogenes*, *Salmonella* and norovirus [2]. An increased number of outbreaks of foodborne illness related with fresh produces has been reported [3]. Consequently, these risks pose a challenge for the food industry [4]. For the preservation of minimally-processed fruits and vegetables, chlorine is used as the most traditional control measure [5]. However, formation of carcinogenic chlorinated organic compounds is suspected in the use of chlorine in water and it is strongly restricted/forbidden in countries in the European Union [6]. Other commonly-used methods such as thermal processing (dry heat or steam), modified atmosphere packing and irradiation are reported to have disadvantages of such as being costly and loss of quality attributes including color loss, flavor changes, vitamin degradation and essential oil loss [7]. The aforementioned drawbacks of conventional disinfection methods have prompted the industries and producers to explore alternative preservation technologies. In this scenario, non-thermal plasma (NTP) stands out as an innovative and promising method that is a dry and no-heat treatment method, with low cost and limited impact on nutritional value and sensory qualities [7, 8].

Abbreviations: FTIR, Fourier transformation infrared spectroscopy; **HNO_3**, nitric acid; MFC, mass flow controller; MWP, microwave-induced plasma; **N_2O_4**, dinitrogen tetroxide; NO, nitrogen monoxide; **NO_2**, nitrogen dioxide; **NO_x**, nitrogen oxides; NTP, non-thermal plasma; PPA, plasma processed-air; PTFE, polytetrafluoroethylene; RNS, reactive nitrogen species; ROS, reactive oxygen species; SIE, specific input energy; SLM, standard litre per minute.

This is an open access article under the terms of the Creative Commons Attribution-NonCommercial-NoDerivs License, which permits use and distribution in any medium, provided the original work is properly cited, the use is non-commercial and no modifications or adaptations are made.

© 2025 The Author(s). *Plasma Processes and Polymers* published by Wiley-VCH GmbH.

Many previous studies have highlighted the strong antimicrobial efficiency of NTP [9–11]. Nonetheless, despite the high potential [12], the further development and large-scale application of NTP technologies in the food industries face challenges due to the complex nature of plasma [1]. The lack of scientific knowledge on the physical and chemical processes' differences in upscaling degrees inhibits the transfer from lab to industry [13]. For example, different sizes of plasma sources, different level of gas flow and absorbed power may lead in consequent to different chemical compositions generated [14]. The effectiveness and impact of NTP in food applications are determined by the reactive species produced through ionization, which are influenced by the gas composition and processing parameters applied. Plasma sources are most easily operated with noble gases such as argon (Ar) and helium (He) [15]. Yet, these gases are in most cases too expensive to be of practical applicability in food production. It is therefore of high interest to promote the development of NTP that can be operated using ambient air as working gas, in which reactive nitrogen species (RNS) and reactive oxygen species (ROS) play critical role in microbial inactivation [16, 17].

An air-operated non-thermal plasma jet used in the study of Hao et al., could produce at maximum 1000 ppm of nitic oxide (NO) at the lowest flow rate of 0.25 slm, along with neglectable concentrations of nitric dioxide (NO_2) and ozone (O_3) [18]. Moiseev et al. have achieved delivering, with a large gap dielectric barrier discharges (DBD) in humid air, around 5600 ppm of O_3 and 1000 ppm of NO_2 under optimal conditions [19]. Above-mentioned examples are typical non-thermal plasmas. However, the maximum concentrations of NO and NO_2 are obtained at around 3500 and 3000 K, respectively, in the equilibrium composition of air [20], which are within the temperature ranges of translational plasmas. These types of high-temperature discharge plasmas such as gliding arc, plasma torch and microwave-driven plasmas have the advantage of a higher electron density that would favor the formation of reactive species. The concentrations of both NO and NO_2, generated by a spark-like discharges in the study of Pavlovich et al., reached at maximum around 6000 ppm with 98% glow power percentage [21]. The maximum concentration of NO_x was 4512 ppm at 90 W input energy at an air flow rate of 6 L/min with a microwave plasma system in the study of Kim et al. [22]. Notably, a peak NO_x production of ~5% was achieved with N_2/O_2 50/50 mixture in the study of Kelly et al., for the purpose of nitrogen fixation [23].

Based on the above, the focus of this study was microwave-induced plasma (MWP) that can be operated at atmospheric pressure with the application of ambient air as carrier gas. Due to the complexity of the chemical composition of air, the resulting chemical interactions are quite complicated and are dependent on various environmental elements such as pressure, temperature and relative humidity. This study aims to both physically and chemically characterize the MWP and to find out its optimal operational conditions for NO_x production. Considering the high temperature in the MW source, an indirect treatment design was made via the plasma-processed-air (PPA). The primary purpose was to firstly find out the main long-living reactive species in PPA. The following hypothesis was that gas relative humidity, input power and flow rate have significant impact on the production of these reactive species among other physiochemical parameters such as electrodes' configuration, operational time and temperature. A fitting model was built, relating the specific energy input and the concentrations of chemical species produced, in an aim to give an fast estimation of targeted concentrations for an up-scaling process and practical applications. This study provides fundamental and essential knowledge for the optimization of plasma treatment to improve microbial inactivation and eventually contribute in the upscaling processes for industrial applications.

2 | Materials and Methods

2.1 | Plasma Source

The microwave-induced plasma used in this study was produced without electrodes and was operated at room temperature and atmospheric pressure. The system usually consists of a solid-state microwave generator typically at 2.45 GHz, a rectangular waveguide, microwave supply and a gas supply (Figure 1a). The plasma source works with electromagnetic waves that are emitted and guided by a coaxial cable (RG 213) to a chamber, where the electrons of gas molecules absorb microwaves and are accelerated, leading to ionization reactions that release energy in the form of UV and visible light photons [15]. As a result, plasmas are formed. Based on this principle, the MidiPLexc (Figure 1b), a microwave-driven plasma source using air as working gas was developed in-house at Leibniz Institute for Plasma Science and Technology (INP; Greifswald, Germany) and was previously introduced in the study of Handorf et al. [17].

The 2.45 GHz microwave generator used (PlasMaster PCU-L 250.3, Heuermann HF-Technik GmbH, Aachen, Germany) can provide an output power between 10 W to 250 W and measure the reflected power that is not absorbed by the plasma source. The working gas from the in-house compressed air supply with a relative humidity of 6.1% is regulated by a mass flow controller (MFC; 1179 C, MKS Instruments Deutschland GmbH, Munich, Germany), whose output unit is standard litre per min (SLM; 1 SLM = $1.67*10^{-5}$ m^3/s). One set of technical operating parameters of MidiPLexc is summarized in Table 1 as an example.

2.2 | Chemical Characterization of Plasma Processed Air (PPA) via FTIR Spectroscopy

Fourier transformation infrared spectrometer (FTIR spectrometer; Vertex 70 v, Bruker, Billerica, MA, USA) was applied to characterize the long-living chemical components present in PPA, whose detector covered a spectral range from 250 to 12 000 cm^{-1}. The measurements were carried out 1.5 m downstream the plasma source—MidiPLexc (Figure 2), with an absorption path length of 0.25 m and a resolution of 0.6 cm^{-1} with eight scans for each measurement. The background spectra of FTIR were taken with the same airflow without the plasma source being ignited. A wavenumber range of 4000–400 cm^{-1} was selected to generate simulated standard spectra. The following vibrational bands were selected for

16128869, 0, Downloaded from https://onlinelibrary.wiley.com/doi/10.1002/ppap.70092 by Cochrane Greece, Wiley Online Library on [16/11/2025]. See the Terms and Conditions (https://onlinelibrary.wiley.com/terms-and-conditions) on Wiley Online Library for rules of use; OA articles are governed by the applicable Creative Commons License

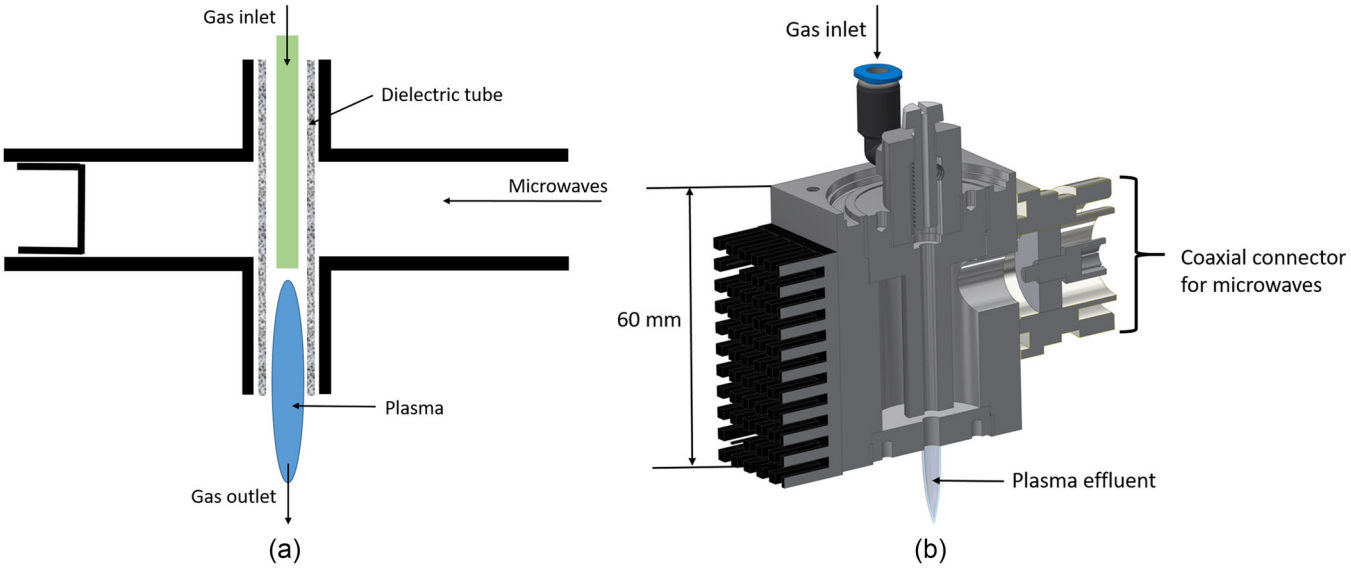

FIGURE 1 | (a) Schematic drawing of a simplified microwave plasma source; (b) Cross section of MidiPLexc.

TABLE 1 | Operation parameters of MidiPLexc.

Technical operating parameters				
Frequency (GHz)	**Power set point (W)**	**Reflected power (W)**	**Reflection (%)**	**Volume flow (SLM)**
2.45	50–80	1.2	2.5	1.5

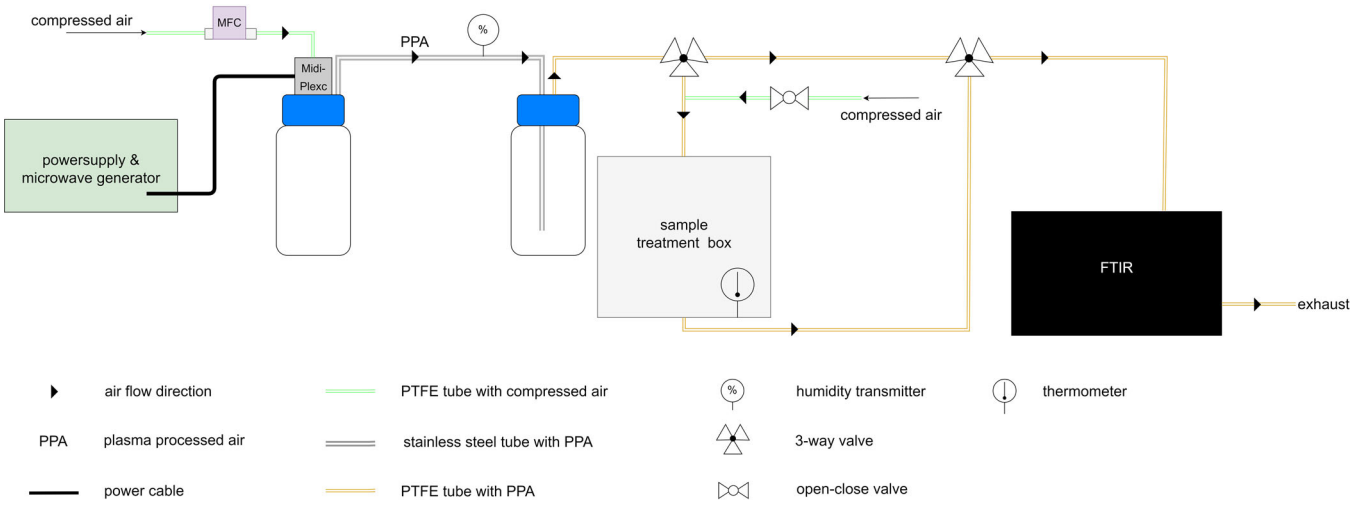

FIGURE 2 | Schematic illustration of the experimental setup with MidiPLexc.

the identification of the presence of chemical compounds based on bands observed from respective reference gases (Linde GmbH, Gases Division, Pullach, Germany): from 1958 to 1787 cm^{-1} for nitrogen oxide (NO), 2919 and 1630 cm^{-1} for nitrogen dioxide (NO_2), 1751 and 1263 cm^{-1} for dinitrogen tetroxide (N_2O_4), 1700 and 1325 cm^{-1} for nitric acid (HNO_3). The peak clusters in the ranges of 4047–3393 cm^{-1} and 2092–1260 cm^{-1} characterized water (H_2O) bands. The absolute concentrations of chemical compounds were calculated from the calibration curves made with respective standard reference gases, by the integrals of respective peaks (from 1958 to 1787 cm^{-1} for NO and from 2940 to 2840 cm^{-1} for NO_2).

2.3 | Experimental Setup

Compressed air was first regulated by the mass flow controller (MFC) to the desired flow rate (Figure 2). PPA was produced via letting compressed air pass the plasma source in the first glass bottle, where water could be added to humidify the system. The humidity was monitored by a humidity transmitter (testo 6651, Testo SE & Co. KGaA, Titisee, Germany). Then the PPA effluent was directed into a second bottle where it stabilized. A treatment chamber was built (Wageningen Food & Biobased Research, Wageningen University & Research,

16128869, 0, Downloaded from https://onlinelibrary.wiley.com/doi/10.1002/ppap.70092 by Cochrane Greece, Wiley Online Library on [16/11/2025]. See the Terms and Conditions (https://onlinelibrary.wiley.com/terms-and-conditions) on Wiley Online Library for rules of use; OA articles are governed by the applicable Creative Commons License

Wageningen, The Netherlands) out of polytetrafluoroethylene (PTFE) with dimensions $15 \times 15 \times 10\ cm^3$, for placing samples, where a thermometer (testo 735, Testo SE & Co. KGaA, Titisee, Germany) was installed inside to allow monitoring of the temperature variations inside during plasma operations. Petri dishes and/or food samples can be placed in this treatment chamber for the indirect treatment by PPA. Thanks to the parallel flow path connecting the PTFE treatment chamber, the main stream of PPA supply was not disturbed while exchanging samples. Subsequently, long-living chemical species produced by microwave plasma that were in stable state in PPA were measured by FTIR spectrometer and lastly were directed to the exhaust.

2.4 | Specific Input Energy (SIE)

The specific input energy describes the energy available for the molecules in the carrier gas in average, which can provide information for the analysis of physical-chemical reactions such as excitation, dissociation and ionization in non-thermal plasmas [24]. According to its definition [25], it was calculated in this study as Equation (1).

$$\text{SIE [J/L]} = \frac{\text{Input power (W)}}{\text{gas flow rate (slm)}/60} = \frac{\text{Input power (J/s)}}{\text{gas flow rate (L/s)}} \quad (1)$$

3 | Results and Discussions

3.1 | Chemical Characterization of Plasma Processed Air (PPA)

In this study, before and during microwave plasma (MWP) ignition, the whole setup was continuously flushed with ambient air, which is a huge advantage to reduce operational cost for large-scale applications. As nitrogen (N_2) and oxygen (O_2) takes up more than 99% of air among all atmospheric constituent [26], the production of RNS and ROS may be expected in most air plasmas [17]. In the current setup, only long-living species in PPA in the downstream were detected by FTIR spectrometer. As shown in Figure 3a, the main chemical compounds in stable state produced by MidiPLexc were found to be primarily NO, followed by NO_2 and N_2O_4. The peak areas' temporal evolution indicates the concentration changes of above-mentioned species. Within the first minute, the concentrations of NO and NO_2 reached 151 and 278 ppm, respectively. The concentration of NO increased to 354 ppm after 5 min, then steadily to 429 ppm after 10 min and finally stabilized in the range of 576–723 ppm after 25 min. In the meantime, the concentration of NO_2 increased more drastically and reached 1575, 2737, and 5382 ppm at 5, 10, and 25 min respectively, without taking into account the concentration of the dimer form N_2O_4. Notably, the gas composition in PPA was dominated by NO_2 by more than an order of magnitude over NO after 10 min. When water vapor was present (100% relative humidity) in the system, additional bands that characterized HNO_3 were observed in the spectra (Figure 3b), which were partially overlapping with those of N_2O_4. Errors were calculated from the standard deviations of three repeated measurements. The errors in percentage for the above-mentioned values for NO and NO_2 were in the range of ±4.3% and ±6.4%, respectively.

These NO_x productions went through a complex series of reactions. Several mechanisms contribute to the generation of these chemical species. Key reactions (R1-8) that are closely related to the generation of these compounds by MidiPLexc are hypothesized based in literature [18, 20, 21, 27] and are illustrated in Figure 4. After MWP ignition, electrons of gas molecules absorbed microwaves and were accelerated [28], leading to dissociation of O_2 into atomic oxygen (**R1**) and excitation of molecular nitrogen to excited state N_2* (**R2**). N_2* immediately reacts with atomic oxygen to form NO and excited/ground-state N (**R3**). Subsequently, N_2* reacts with O_2 to form more NO and

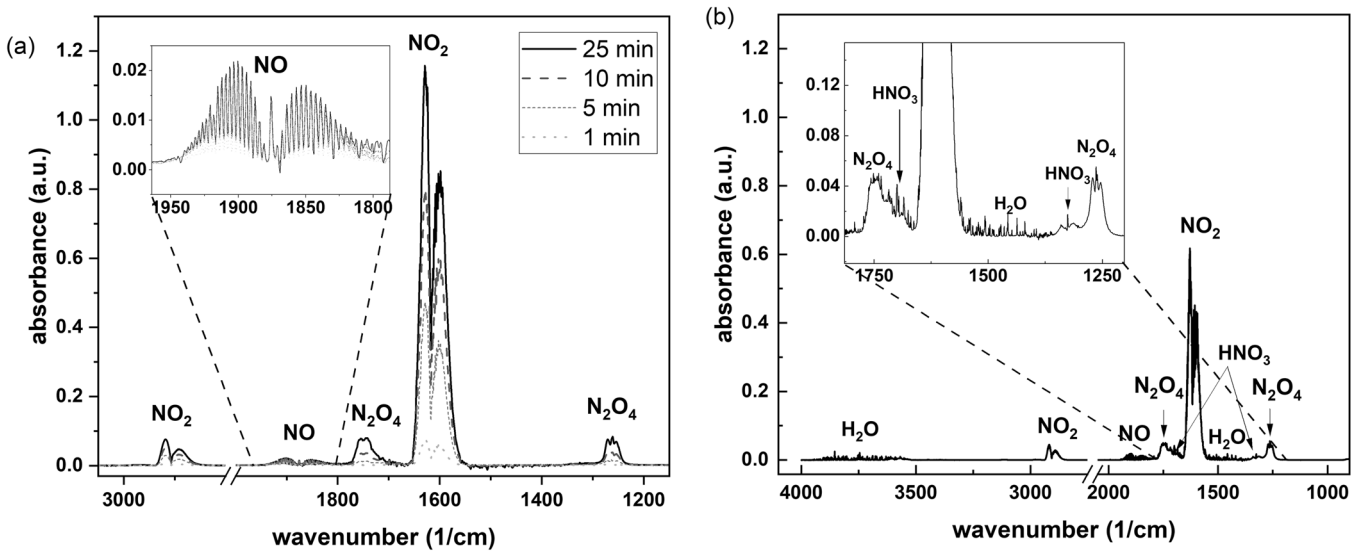

FIGURE 3 | (a) FTIR spectra showing the temporal evolution of NO, NO_2 and N_2O_4 in PPA under dry conditions (dew point −14.5°C). Power set point was 50 W and flow rate was 1.5 SLM. An enlarged view of the absorbance bands of NO was given at top-left. (b) FTIR spectra indicating the presence of H_2O and HNO_3 in addition to NO, NO_2 and N_2O_4 in PPA under wet condition (100% RH). Power set point was 50 W and flow rate was 1.5 SLM. An enlarged window for the wavenumber range 1814–1200 cm^{-1} was given at the top-left.

16128869, 0, Downloaded from https://onlinelibrary.wiley.com/doi/10.1002/ppap.70092 by Cochrane Greece, Wiley Online Library on [16/11/2025]. See the Terms and Conditions (https://onlinelibrary.wiley.com/terms-and-conditions) on Wiley Online Library for rules of use; OA articles are governed by the applicable Creative Commons License

O (**R4**). Based on the preliminary results obtained in the studies of Ehlbeck et al. and Baeva et al. [29, 30], the gas temperature in the core of MWP source is estimated to achieve from 2000 K to 3000 K. As a result, the plasma is close to thermodynamic equilibrium and its chemical composition is best described in the model developed by Ammann and Timmins [20]. For this temperature region, beside N_2 and O_2, NO is the main component. The formation of NO_2 takes place during the temperature drop after the active plasma zone. Ozone generation is often expected in air plasmas [28]. However, no trace of O_3 was detected at all by FTIR spectrometer during the whole plasma operation of MidiPLexc. It is assumed that in this case it was either consumed in the reaction with NO to form NO_2 or was probably in contact with the inside surface of the tubes before reaching the measurement gas cell of FTIR spectrometer which was 1.5 m downstream the plasma source.

$$O_2 + e^- \rightarrow O + O + e^- \quad \text{(R1)}$$

$$N_2 + e^- \rightarrow N_2^* + e^- \quad \text{(R2)}$$

$$N_2^* + O \rightarrow NO + N^* \quad \text{(R3)}$$

$$N^* + O_2 \rightarrow NO + O \quad \text{(R4)}$$

$$NO{+}O + M \rightarrow NO_2 + M \quad \text{(R5)}$$

$$2NO + O_2 \rightarrow 2NO_2 \quad \text{(R6)}$$

$$2NO_2 + M \leftrightarrow N_2O_4 + M \quad \text{(R7)}$$

$$3NO_2 + H_2O \leftrightarrow 2HNO_3{+}NO \quad \text{(R8)}$$

Considering the way greater concentration (more than an order of magnitude) of NO_2 than NO observed in PPA, **Reaction 5** & **6** are hypothesized to be the main reactions for consumption of NO and for the production of NO_2. This finding is consistent with that of Kim et al. [22], who found that NO_2 concentration was about 21 times higher than that of NO at input power of 90 W with a microwave plasma system. However, in other type of plasma sources such as the non-thermal plasma jet used in the study of Hao et al. [18], NO was found to be the dominant long-living product where concentration of NO_2 was negligible at all different flow rates (1–8 SLM). In Hao et al.'s study, NO_2 could only be detected at the lowest investigated power at 0.60 W for all the three nozzles tested. Simultaneously, NO_2 exists in equilibrium with its dimer—N_2O_4 (**R7**), in microseconds [31]. According to Chao et al. [32], for current investigated experimental conditions, the concentration of N_2O_4 can be calculated via the equilibrium constant of 0.136 in relation to NO_2 at room temperature. Under humid conditions when water molecules were available, part of NO_2 gas was absorbed and small amount of HNO_3 was produced (**R8**).

These reported reactive species are important for both gaseous and liquid application for antimicrobial measures. For example, the dominant component of PPA-NO_2 has been reported to be capable of inducing lipid peroxidation, resulting in membrane rupture and cell death [33]. The analysis of bacterial inactivation by PPA has been thoroughly investigated in a separate study of Battaggia et al. [16] with the same setup with MidiPLexc. Conclusively, bacterial vegetative cells and yeast were effectively inactivated after a 60 s-PPA treatment in an agar plate model system, with an average reduction from 4.9 $\log_{10}$ to 5.9 $\log_{10}$, with limited strain variability. Schnabel et al. have theoretically supposed the possible impact of RNS and ROS on bacteria on different cell levels in more detailed [34]. The study of Barkhade et al. provided a further comprehensive insight into the bacterial inactivation mechanism in the aspects of membrane impairment and DNA damage under the direct treatment of MW plasma [35].

3.2 | The Influence of Flow Rate on NO_x Concentration in PPA

The concentration of NO in PPA was not much influenced by flow rate changes with only minor fluctuations in the range of

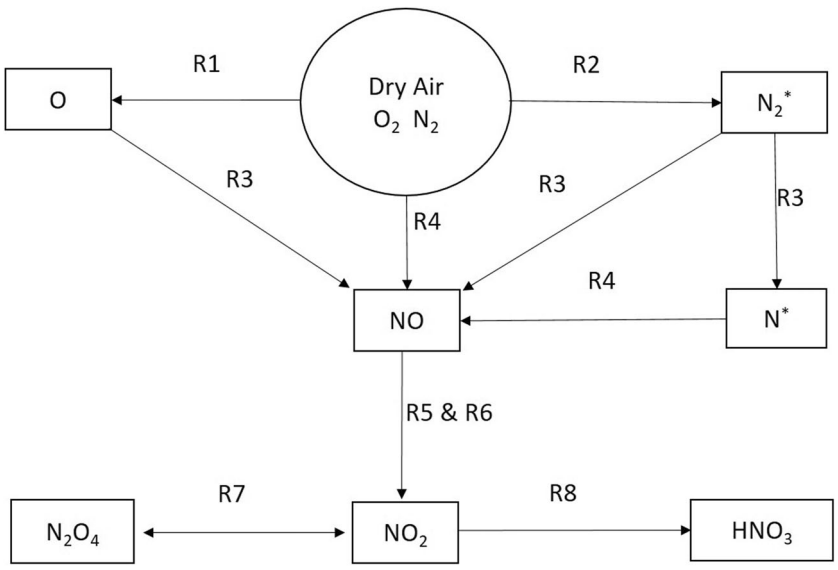

FIGURE 4 | Diagram of primary chemical reactions in dry air plasma by MidiPLexc, following electron-impact on N_2 and O_2. The asterisk (*) denotes an excited state and M denotes natural molecules.

16128869, 0, Downloaded from https://onlinelibrary.wiley.com/doi/10.1002/ppap.70092 by Cochrane Greece, Wiley Online Library on [16/11/2025]. See the Terms and Conditions (https://onlinelibrary.wiley.com/terms-and-conditions) on Wiley Online Library for rules of use; OA articles are governed by the applicable Creative Commons License

753-957 ppm when the flow rate of carrier gas—air was changed from 1.0 to 2.0 SLM (Figure 5). Based from that, a linear relationship can be deducted between the number of NO molecules and flow rate.

Differently, the flow rate had a stronger impact on the concentration of NO_2, that increased from 8441 to 9047 ppm while the flow rate increased from 1.0 to 1.5 SLM. After 1.5 SLM, the concentration of NO_2 decreased to 8080 and 7592 ppm at flow rate 1.75 and 2.0 SLM respectively. Maximum concentration of NO_x (sum of NO and NO_2) was found at the flow rate of 1.5 SLM for the configuration of MidiPLexc. The number of NO_2 molecules went through a steeper increase as the flow rate increased from 1.0 to 1.5 SLM and tended to reach a limit at 1.5 SLM. When the flow increased above 1.5 SLM, the dilution of the NO_2 molecules with the increased flowrate was greater than the increased number of the molecule production, resulting a decrease in concentration. As concentration is the key to microbial inactivation in a closed environment, all experiments were therefore executed with a flow of 1.5 SLM for the highest concentration of NO_2, which was determined to be the critical flow rate for the configuration of MidiPLexc and this point needs to be taken into account for the upscaling process. Increased flow rates were often only reported to have a negative impact on the NO_x concentration [18, 22], due to the unawareness of the existence of critical flow rate for the maximum concentration discovered in this study.

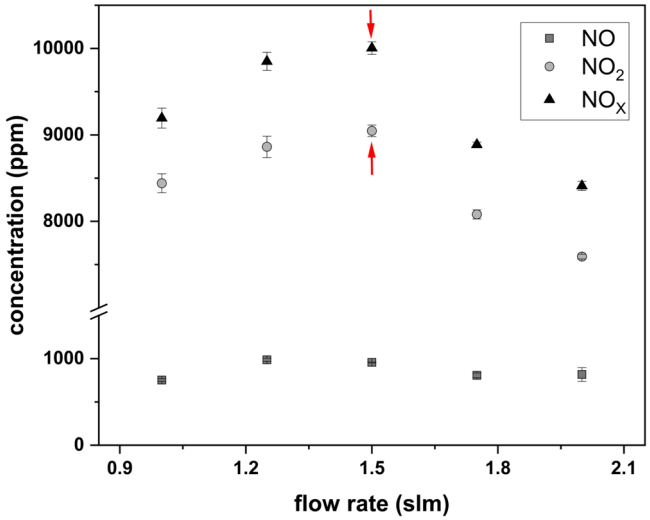

FIGURE 5 | Concentrations of NO, NO_2 and their sum NO_x as a function of flow rate, under dry condition and power set point 80 W. The error bars represent standard deviations from three repeated measurements. The errors in percentage for the above-mentioned values for NO and NO_2 were in the range of ±9.7% and ±1.4%, respectively. The arrows indicate the concentrations of NO_2 and NO_x at critical flow rate 1.5 SLM.

3.3 | The Influence of Power on NO_x Concentration in PPA

Firstly, the plasma source could not be ignited or the plasma flame could not be maintained for the power set point below 40 W. Evolution of concentrations during a 60 min' plasma source operation was monitored, except for 100 W, as the power supply went down after 40 min due to internal overheating. For the first 40 min, the concentrations of NO_2 increased steadily for all different power set points under dry conditions and started to stabilize from 40 min (Figure 6a). From the tendency, it was estimated that the concentration of NO_2 would stabilize and reach a maximum for the respective power set point, which was approximately 6806, 7640, 7701, 8741, and 9995 ppm for 40, 50, 60, 70, and 80 W respectively. The maximum production of NO_2 reached 10 528 ppm at 90 W. However, when compared with the dry condition at the same power set point 50 W, the concentration of NO_2 was reduced by approximately 41% under 100% relative humidity. A shorter stabilization time (25 min) of NO_2 in the gas phase was noticed under humid condition. It has been reported that high relative gas humidity (RH 70%) increased

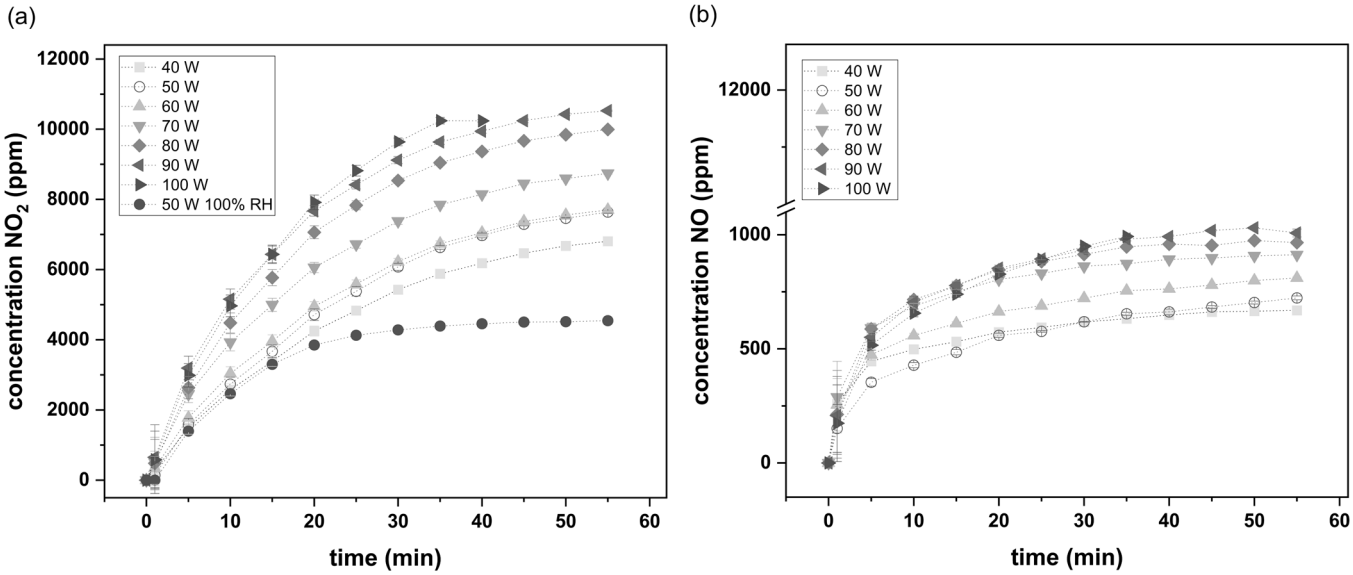

FIGURE 6 | Temporal evolution of the concentrations of NO_2 (a) and NO (b) in PPA under different power settings when the gas flow rate was fixed at 1.5 SLM. The dotted lines only serve to connect data points to visualize the tendency. The error bars represent standard deviations from three repeated measurements.

16128869, 0, Downloaded from https://onlinelibrary.wiley.com/doi/10.1002/ppap.70092 by Cochrane Greece, Wiley Online Library on [16/11/2025]. See the Terms and Conditions (https://onlinelibrary.wiley.com/terms-and-conditions) on Wiley Online Library for rules of use; OA articles are governed by the applicable Creative Commons License

TABLE 2 | Summary of power reflection of MidiPLexc at different power set points.

Power set point	40 W	50 W	60 W	70 W	80 W	90 W	100 W
Reflected power	1.0 W	0.9 W	5.5 W	6.7 W	9.0 W	12.0 W	14.0 W
Reflection (%)	2.4%	2.3%	9.4%	10.0%	11.2%	13.1%	13.9%

the mortality of *Aspergillus niger* spores by a low temperature plasma [36]. Unfortunately, FTIR spectroscopy applied in this study was not appropriate to quantify gaseous nitric acid in humidified PPA for further analysis. Other techniques available in the market, such as UV-visible absorbance spectroscopy and ion chromatography used in previous studies [21, 37], were used only for the characterization of nitrite and nitrate in aqueous phase. Additional work is needed to develop suitable analytical instruments for further investigations, especially for the after-flow gas phase of non-thermal air plasmas under humidified conditions. On the other hand, the concentrations of NO developed differently as the power set point increased compared with those of NO_2 (Figure 6b). All the concentrations started to stabilize at 10 min, and were approximately 669, 723, 810, 912, 975, and 1030 ppm for 40, 50, 60, 70, 80, and 90 W respectively.

Three factors are considered to be accountable for the temporal evolution (i.e., increase) of the concentration of the chemical species in PPA. Firstly, the remaining moisture in the compressed air absorbed certain microwave energy at beginning of plasma source operation. Additionally, it took approximately 5 min for the effluent of PPA under 1.5 SLM flow rate to pass through and stabilize in the 1 L-bottle, the treatment chamber and the tubes and finally reach the FTIR spectrometer. Mainly, certain time was required to reach the steady state conditions for plasma generation. For example, the warming-up time for the bottles and tubes to reach the effluent temperature was around 20 min. This point needs always to be taken into account for future operations, as the reactions **R5**, **R6**, and **R7** are known to be temperature-sensitive [20, 32].

As expected, the NO_x concentrations increased as the input power increased, due to the higher number of electrons, ions and the collisions in-between, similar to what was reported in previous studies [21, 22]. However, unlike the continuous increasing concentration of NO_2 along with the increasing input power, the concentration of NO remained relatively constant after 20 min of stabilization time. These results confirm that reactions (**R5** & **R6**) were the dominant ones, converting NO into NO_2. It is thus concluded that the elevated input power mainly promotes NO_2 generation by MidiPLexc.

As such the above results provide a possible explanation on why dissipated power was found to be the most correlated parameter for the inactivation efficacy of non-thermal plasma antimicrobial treatment, following a meta-analysis [38].

3.4 | Prediction Model for Concentration of NO_x Produced

Certain output power was not consumed by the microwave plasma source (MidiPLexc) and reflected back to the power supply. The reflection rates at different power set points are summarized in Table 2. There was a tendency of increasing reflection rate with increasing power set point.

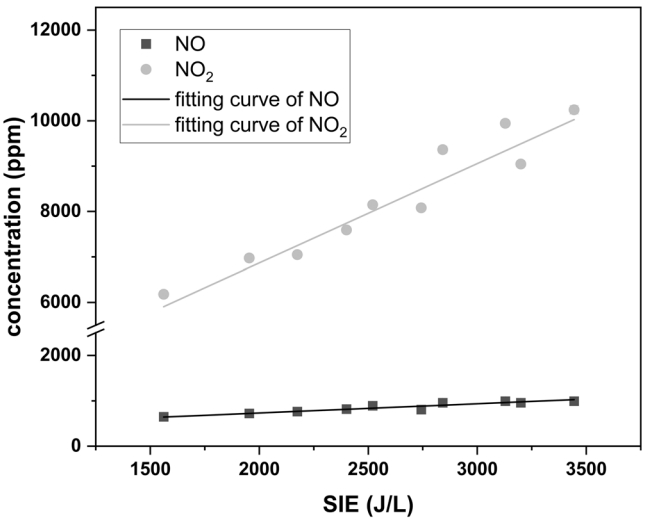

FIGURE 7 | Concentrations of NO and NO_2 as a function of specific input energy (SIE) and their respective fitting curves. The error bars represent standard deviations from three repeated measurements, which were rather small and difficult to see in the figure due to scales. The equation of the linear fitting curve of NO is: $y = 0.20x + 323.10$, $R^2 = 0.92$. The equation of the linear fitting curve of NO_2 is: $y = 2.19x + 2491.70$, $R^2 = 0.91$.

The relationship between species' concentration and specific input energy (SIE) calculated by Equation (1), is presented in Figure 7, where the reflected power was factored out of the input power in the calculations of SIE. In general, the concentration of NO fluctuated slightly within the range of 649–992 ppm while the SIE increased. As a result, a simple prediction model for estimation of the concentration of NO is expressed as below:

$$\text{Concentration of NO [ppm]} = 0.20 * \text{SIE} + 323.10 \quad (2)$$

Of which, the coefficient of determination is 0.92.

In contrast, the concentration of NO_2 increased from 6182 to 10 243 ppm while the SIE increased from 1562 to 3444 J/L. SIE values resulted from the calculation with flow rates below the critical one (1.5 SLM) were not included into the regression. The prediction model for the estimation of concentration of NO_2 is expressed as below:

$$\text{Concentration of NO2 [ppm]} = 2.19 * \text{SIE} + 2491.70 \quad (3)$$

16128869, 0, Downloaded from https://onlinelibrary.wiley.com/doi/10.1002/ppap.70092 by Cochrane Greece, Wiley Online Library on [16/11/2025]. See the Terms and Conditions (https://onlinelibrary.wiley.com/terms-and-conditions) on Wiley Online Library for rules of use; OA articles are governed by the applicable Creative Commons License

Of which, the coefficient of determination is 0.91.

With the help of the prediction models of NO_x production via MidiPLexc realized in this study, estimations of concentrations of NO and NO_2 in PPA for various applications can be made easily without sophisticated and costly analytical instruments. The prediction models made in this study indicated a linear dependency of both NO and NO_2 on specific input energy (SIE), which makes the SIE a key design parameter for the up-scaling processes. However, it is critical to only apply these models for the concentrations below 10 000 ppm to stay within the linear range. One of the reasons is due to the reversible dimerization reaction of NO_2 to N_2O_4, which has been discussed previously. More importantly, due to the nonlinearity phenomenon in gas-phase FTIR spectroscopy for high concentrations [39].

3.5 | Temperature Variation During Microwave Plasma Operation

During 25 min of plasma source operation, the temperature which was monitored inside the PTFE treatment chamber stabilized at approximately 21.5°C (Figure 8). In comparison, the room temperature outside the chamber fluctuated slightly from 19.1°C to 20.9°C. The difference between inside and outside was within 2.4°C and both were considered within the range of room temperature (20°C–25°C).

Very few studies of plasma experiments have reported the temperature at the exhaust of the plasma gas effluent, mainly focused on the temperature in the core of plasma [15, 28]. In this study, the temperature at the gas outlet inside the treatment box was measured, which was with limited variations within the range of room temperature during all the plasma operations. This result provides support for MW plasma to be applied as a non-thermal treatment method for food.

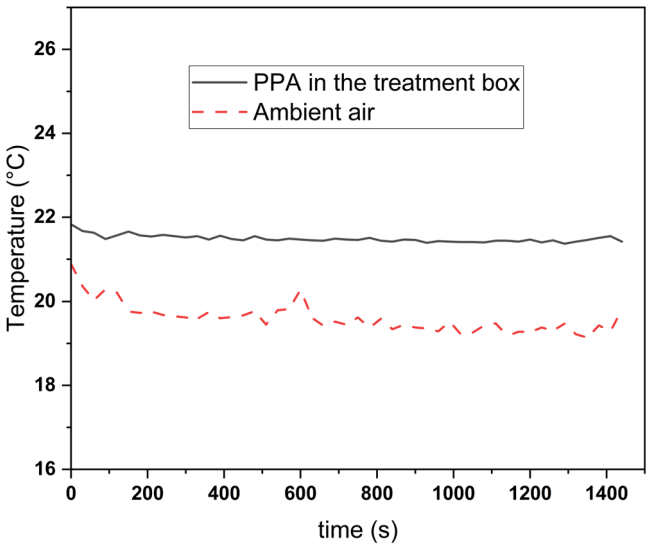

FIGURE 8 | Temporal evolution of temperature inside (black continuous line) and outside (red dotted line) the PPA treatment chamber (position see in Figure 2).

4 | Conclusions

This study shows that MWP source is able to deliver high concentration of antimicrobial compounds such as NO and NO_2 with low input energy, among which NO_2 is the dominant compound by more than an order of magnitude over NO. It was proven that humidity, flow rate and input power have significant impact on the production of NO_2. These parameters need to be carefully taken into account for the upscaling of plasma source that could deliver a larger volume of PPA to pilot scale. Overheating shall be avoided when working with a stronger power supply.

The prediction models made in this study can serve as a fast and non-costly method for the estimation of NO_x concentration while altering the parameters for upscaling. A group of datasets shall be collected via FTIR spectrometer with the upscaled equipment to validate the robustness of the models for future wider application in industrial scenarios, such as to reach the targeted concentrations by controlling the specific input energy.

With the possibilities to be operated under ambient pressure and with atmospheric air, which significantly reduce the equipment and operational costs, the MW plasma shows its economic viability and huge potential in large scale applications in food industries. Furthermore, this type of treatment takes place under room temperature and thus induces minimal impact on food quality. The dry treatment with PPA also preserves better the flavor and fragrance of the food products that are more vulnerable to lose under washing processes.

Author Contributions

Yijiao Yao: conceptualization, data curation, formal analysis, investigation, methodology, visualization, writing – original draft. **Thomas Weihe:** funding acquisition, visualization, writing – review and editing. **Jörg Stachowiak:** resources, software, visualization, writing – review and editing. **Jörg Ehlbeck:** conceptualization, formal analysis, funding acquisition, methodology, project administration, supervision, writing – review and editing. **Uta Schnabel:** conceptualization, funding acquisition, project administration, supervision, writing – review and editing. **Kimon-Andreas Karatzas:** conceptualization, funding acquisition, supervision, writing – review and editing.

Acknowledgments

The authors would like to acknowledge Remco Hamoen (Wageningen Food & Biobased Research, Wageningen University & Research, Wageningen, The Netherlands) for the design of the treatment chamber. This study is part of the TRANSIT project and has received funding from the European Union's Horizon 2020 research and innovation program under the Marie Skłodowska-Curie grant agreement N°955431. Additionally, funding has been received from the Federal Republic of Germany, Federal Ministry of Education and Research under the program "PlaVir," and funding reference: 03COV05A. Further funding for the work has been provided by the Federal Republic of Germany and the country's State Mecklenburg-Western Pomerania, Ministry of Science, Culture, Federal and European Affairs under the grant agreement N° VIII-0639-INP00-2023/004-002.

Data Availability Statement

The data that support the findings of this study are available from the corresponding author upon reasonable request.

16128869, 0, Downloaded from https://onlinelibrary.wiley.com/doi/10.1002/ppap.70092 by Cochrane Greece, Wiley Online Library on [16/11/2025]. See the Terms and Conditions (https://onlinelibrary.wiley.com/terms-and-conditions) on Wiley Online Library for rules of use; OA articles are governed by the applicable Creative Commons License

References

1. X. Liao, D. Liu, Q. Xiang, et al., "Inactivation Mechanisms of Non-Thermal Plasma on Microbes: A Review," *Food Control* 75 (2017): 83–91, https://doi.org/10.1016/j.foodcont.2016.12.021.

2. A. Fernández, E. Noriega, and A. Thompson, "Inactivation of *Salmonella enterica* Serovar Typhimurium on Fresh Produce by Cold Atmospheric Gas Plasma Technology," *Food Microbiology* 33, no. 1 (2013): 24–29, https://doi.org/10.1016/j.fm.2012.08.007.

3. FAO/WHO, Food and Agriculture Organization of the United Nations/World Health Organization., 2023. Prevention and Control of Microbiological Hazards in Fresh Fruits and Vegetables: parts 1 & 2: General Principles: Meeting Report, https://iris.who.int/bitstream/handle/10665/375591/9789240082083-eng.pdf?sequence=1 (Accessed on 09 June 2024).

4. D. Ziuzina, S. Patil, P. J. Cullen, K. M. Keener, and P. Bourke, "Atmospheric Cold Plasma Inactivation of *Escherichia coli*, *Salmonella Enterica* Serovar Typhimurium and *Listeria monocytogenes* Inoculated on Fresh Produce," *Food Microbiology* 42 (2014): 109–116, https://doi.org/10.1016/j.fm.2014.02.007.

5. J. Adaskaveg, H. Förster, and N. F. Sommer, "Principles of Postharvest Pathology and Management of Decays of Edible Horticultural Crops." *Postharvest Technology of Horticultural Crops, University of California Publication, California* (2002). 331, 163–195.

6. U. De Corato, "Improving the Shelf-Life and Quality of Fresh and Minimally-Processed Fruits and Vegetables for a Modern Food Industry: A Comprehensive Critical Review From the Traditional Technologies Into the Most Promising Advancements," *Critical Reviews in Food Science and Nutrition* 60, no. 6 (2020): 940–975, https://doi.org/10.1080/10408398.2018.1553025.

7. S. Mošovská, V. Medvecká, N. Halászová, et al., "Cold Atmospheric Pressure Ambient Air Plasma Inhibition of Pathogenic Bacteria on the Surface of Black Pepper," *Food Research International* 106 (2018): 862–869, https://doi.org/10.1016/j.foodres.2018.01.066.

8. U. Schnabel, R. Niquet, O. Schlüter, H. Gniffke, and J. Ehlbeck, "Decontamination and Sensory Properties of Microbiologically Contaminated Fresh Fruits and Vegetables by Microwave Plasma Processed Air (PPA): Decontamination and Sensory of Food by Plasma," *Journal of Food Processing and Preservation* 39, no. 6 (2015): 653–662, https://doi.org/10.1111/jfpp.12273.

9. B. G. Dasan, M. Mutlu, and I. H. Boyaci, "Decontamination of *Aspergillus flavus* and *Aspergillus parasiticus* Spores on Hazelnuts via Atmospheric Pressure Fluidized Bed Plasma Reactor," *International Journal of Food Microbiology* 216 (2016): 50–59, https://doi.org/10.1016/j.ijfoodmicro.2015.09.006.

10. B. A. Niemira, G. Boyd, and J. Sites, "Cold Plasma Rapid Decontamination of Food Contact Surfaces Contaminated With *Salmonella* Biofilms," *Journal of Food Science* 79, no. 5 (2014): M917–M922, https://doi.org/10.1111/1750-3841.12379.

11. H. Winter, R. Wagner, Y. Yao, J. Ehlbeck, and U. Schnabel, "Influence of Plasma-Treated Air on Surface Microbial Communities on Freshly Harvested Lettuce," *Current Research in Food Science* 7 (2023): 100649, https://doi.org/10.1016/j.crfs.2023.100649.

12. O. Schlüter, J. Ehlbeck, C. Hertel, et al., "Opinion on the Use of Plasma Processes for Treatment of Foods," *Molecular Nutrition & Food Research* 57, no. 5 (2013): 920–927, https://doi.org/10.1002/mnfr.201300039.

13. S. Ojha, A. Fröhling, J. Durek, et al., "Principles and Application of Cold Plasma in Food Processing," *Innovative Food Processing Technologies, A Comprehensive Review (2021)* (2021): 519–540, https://doi.org/10.1016/b978-0-08-100596-5.23033-3.

14. D. A. Laroque, S. T. Seó, G. A. Valencia, J. B. Laurindo, and B. A. M. Carciofi, "Cold Plasma in Food Processing: Design, Mechanisms, and Application," *Journal of Food Engineering* 312 (2022): 110748, https://doi.org/10.1016/j.jfoodeng.2021.110748.

15. X. Lu, G. V. Naidis, M. Laroussi, S. Reuter, D. B. Graves, and K. Ostrikov, "Reactive Species in Non-Equilibrium Atmospheric-Pressure Plasmas: Generation, Transport, and Biological Effects," *Physics Reports* 630 (2016): 1–84, https://doi.org/10.1016/j.physrep.2016.03.003.

16. D. Battaggia, Y. Yao, M. N. Nierop Groot, T. Abee, and H. M. W. den Besten, "Impact of Species and Strain Variability on Non-Thermal Plasma Decontamination Efficacy," *Innovative Food Science & Emerging Technologies* 95 (2024): 103674, https://doi.org/10.1016/j.ifset.2024.103674.

17. O. Handorf, H. Below, U. Schnabel, K. Riedel, and J. Ehlbeck, "Investigation of the Chemical Composition of Plasma-Treated Water by MidiPLexc and Its Antimicrobial Effect *on L. monocytogenes* and *Pseudomonas fluorescens* Monospecies Suspension Cultures," *Journal of Physics D: Applied Physics* 53, no. 30 (2020): 305204, https://doi.org/10.1088/1361-6463/ab866b.

18. X. Hao, A. M. Mattson, C. M. Edelblute, M. A. Malik, L. C. Heller, and J. F. Kolb, "Nitric Oxide Generation With an Air Operated Non-Thermal Plasma Jet and Associated Microbial Inactivation Mechanisms," *Plasma Processes and Polymers* 11, no. 11 (2014): 1044–1056, https://doi.org/10.1002/ppap.201300187.

19. T. Moiseev, N. N. Misra, S. Patil, et al., "Post-Discharge Gas Composition of a Large-Gap DBD in Humid Air by UV–Vis Absorption Spectroscopy," *Plasma Sources Science and Technology* 23, no. 6 (2014): 065033, https://doi.org/10.1088/0963-0252/23/6/065033.

20. P. R. Ammann and R. S. Timmins, "Chemical Reactions During Rapid Quenching of Oxygen-Nitrogen Mixtures From Very High Temperatures," *AIChE Journal* 12, no. 5 (1966): 956–963, https://doi.org/10.1002/aic.690120522.

21. M. J. Pavlovich, T. Ono, C. Galleher, et al., "Air Spark-Like Plasma Source for Antimicrobial NOx Generation," *Journal of Physics D: Applied Physics* 47, no. 50 (2014): 505202, https://doi.org/10.1088/0022-3727/47/50/505202.

22. T. Kim, S. Song, J. Kim, and R. Iwasaki, "Formation of NO_x From Air and N_2/O_2 Mixtures Using a Nonthermal Microwave Plasma System," *Japanese Journal of Applied Physics* 49, no. 12R (2010): 126201, https://doi.org/10.1143/JJAP.49.126201.

23. S. Kelly and A. Bogaerts, "Nitrogen Fixation in an Electrode-Free Microwave Plasma," *Joule* 5, no. 11 (2021): 3006–3030, https://doi.org/10.1016/j.joule.2021.09.009.

24. D. Hegemann, "Plasma Activation Mechanisms Governed by Specific Energy Input: Potential and Perspectives," *Plasma Processes and Polymers* 20, no. 5 (2023): e2300010, https://doi.org/10.1002/ppap.202300010.

25. K. Salonitis, J. Paralikas, A. Fysikopoulos, and G. Chryssolouris, "Specific Energy." in *CIRP Encyclopedia of Production Engineering*, eds. L. Laperrière and G. Reinhart (2014), 1124–1128, https://doi.org/10.1007/978-3-642-20617-7_16776.

26. C. W. Allen, *Astrophysical Quantities* (1976). (3rd ed.), 119.

27. I. A. Kossyi, A. Y. Kostinsky, A. A. Matveyev, and V. P. Silakov, "Kinetic Scheme of the Non-Equilibrium Discharge in Nitrogen-Oxygen Mixtures," *Plasma Sources Science and Technology* 1, no. 3 (1992): 207–220, Article 011, https://doi.org/10.1088/0963-0252/1/3/011.

28. J. Meichsner, M. Schmidt, R. Schneider, and H.-E. Wagner, *Nonthermal Plasma Chemistry and Physics* (2013), 7–8.

29. J. Ehlbeck, R. Brandenburg, T. von Woedtke, U. Krohmann, M. Stieber, and K. D. Weltmann, "PLASMOSE - Antimicrobial Effects of Modular Atmospheric Plasma Sources," *GMS Krankenhaushygiene interdisziplinar* 3, no. 1 (2008): 14.

16128869, 0, Downloaded from https://onlinelibrary.wiley.com/doi/10.1002/ppap.70092 by Cochrane Greece, Wiley Online Library on [16/11/2025]. See the Terms and Conditions (https://onlinelibrary.wiley.com/terms-and-conditions) on Wiley Online Library for rules of use; OA articles are governed by the applicable Creative Commons License

30. M. Baeva, A. Bösel, J. Ehlbeck, and D. Loffhagen, "Modeling of Microwave-Induced Plasma in Argon at Atmospheric Pressure," *Physical Review E* 85 (2012): 056404, https://doi.org/10.1103/PhysRevE.85.056404.

31. T. van Raak, H. van den Bogaard, F. Gallucci, and S. Li, "The Significance of NO2 Dimerization in Plasma-Based NO Synthesis for Nitrogen Fixation," *Journal of Energy Chemistry* 99 (2024): 522–528, https://doi.org/10.1016/j.jechem.2024.08.013.

32. J. Chao, R. C. Wilhoit, and B. J. Zwolinski, "Gas Phase Chemical Equilibrium in Dinitrogen Trioxide and Dinitrogen Tetroxide," *Thermochimica Acta* 10, no. 4 (1974): 359–371, https://doi.org/10.1016/0040-6031(74)87005-X.

33. R. P. Patel, J. McAndrew, H. Sellak, et al., "Biological Aspects of Reactive Nitrogen Species," *Biochimica et Biophysica Acta (BBA) - Bioenergetics* 1411, no. 2–3 (1999): 385–400, https://doi.org/10.1016/S0005-2728(99)00028-6.

34. U. Schnabel, M. Balazinski, R. Wagner, et al., "Optimizing the Application of Plasma Functionalised Water (PFW) for Microbial Safety in Fresh-Cut Endive Processing," *Innovative Food Science & Emerging Technologies* 72 (2021): 102745, https://doi.org/10.1016/j.ifset.2021.102745.

35. T. Barkhade, K. Nigam, G. Ravi, S. Rawat, and S. K. Nema, "Investigating the Effects of Microwave Plasma on Bacterial Cell Structures, Viability, and Membrane Integrity," *Scientific Reports* 15, no. 1 (2025): 18052, https://doi.org/10.1038/s41598-025-02312-4.

36. P. Muranyi, J. Wunderlich, and M. Heise, "Influence of Relative Gas Humidity on the Inactivation Efficiency of a Low Temperature Gas Plasma," *Journal of Applied Microbiology* 104, no. 6 (2008): 1659–1666, https://doi.org/10.1111/j.1365-2672.2007.03691.x.

37. U. Schnabel, O. Handorf, K. Yarova, et al., "Plasma-Treated Air and Water-Assessment of Synergistic Antimicrobial Effects for Sanitation of Food Processing Surfaces and Environment," *Foods* 8, no. 2 (2019): 55, https://doi.org/10.3390/foods8020055.

38. G. Pampoukis, M. H. Zwietering, and H. M. W. den Besten, "Ranking Factors Affecting the Decontamination Efficacy of Non-Thermal Plasma: The Approach of Dissipated Power Per Plasma Volume Through Machine Learning Modeling," *Innovative Food Science & Emerging Technologies* 96 (2024): 103773, https://doi.org/10.1016/j.ifset.2024.103773.

39. M. Ahro and J. Kauppinen, "Nonlinearity of Beer's Law in Gas-Phase FT-IR Spectroscopy," *Applied Spectroscopy* 55, no. 1 (2001): 50–54, https://doi.org/10.1366/0003702011951425.

16128869, 0, Downloaded from https://onlinelibrary.wiley.com/doi/10.1002/ppap.70092 by Cochrane Greece, Wiley Online Library on [16/11/2025]. See the Terms and Conditions (https://onlinelibrary.wiley.com/terms-and-conditions) on Wiley Online Library for rules of use; OA articles are governed by the applicable Creative Commons License